

Cite this: *RSC Adv.*, 2017, 7, 15455

# Three-dimensional electro-Fenton oxidation of N-heterocyclic compounds with a novel catalytic particle electrode: high activity, wide pH range and catalytic mechanism†

Baolin Hou,\* Bozhi Ren, Renjian Deng, Guocheng Zhu, Zhenghua Wang and Zhi Li

A novel three-dimensional (3D) heterogeneous electro-Fenton (EF) system with sludge derived activated carbon from sewage and iron sludge (SAC-Fe) as catalytic particle electrodes (CPEs) was constructed in this study. Its application in degrading nitrogen-heterocyclic compounds (NHCs) exhibited high catalytic efficiency over a wide applicable pH range from 3.0 to 9.0. SAC-Fe worked as both CPEs and a heterogeneous catalyst in this 3D EF system, enhancing oxidation activity. Degradation pathways of the NHCs (indole, quinoline and pyridine) and reasonable reaction mechanisms involved in this 3D EF were proposed. At pH 3.0, hydroxyl radicals were the dominant participant oxidants, following a Haber–Weiss mechanism. The  $\text{Fe}^{\text{II}}$  sites catalyzed the decomposition of electro-generated  $\text{H}_2\text{O}_2$  to yield  $\cdot\text{OH}$ . At pH 9.0, the oxidants generated from the decomposition of  $\text{H}_2\text{O}_2$  were mainly  $\cdot\text{O}_2^-/\text{HO}_2\cdot$  and to lesser extent were  $\cdot\text{OH}$ . The formation and decomposition of  $\text{H}_2\text{O}_2$  complex with catalytic sites ( $\text{Fe}^{\text{II}}$  and  $\text{Fe}^{\text{III}}$ ) as well as the catalytic decomposition of  $\text{H}_2\text{O}_2$  were involved in the catalytic reactions to generate  $\cdot\text{O}_2^-/\text{HO}_2\cdot$  and  $\cdot\text{OH}$ . A quantitative structure–activity relationship analysis (QSAR) model was developed to describe the relationship between degradation properties of NHCs and their structures by involving quantum descriptors.

Received 10th January 2017  
Accepted 28th February 2017

DOI: 10.1039/c7ra00361g

rsc.li/rsc-advances

## 1. Introduction

Nitrogen-heterocyclic compounds (NHCs) are a group of environmentally significant contaminants, which mainly come from coal gasification, oil processing, coal-tar waste and creosote wood preservation.<sup>1</sup> NHCs are generally water-soluble and NHCs are the main refractory organic pollutants residual in coal gasification wastewater.<sup>2</sup> Many NHCs are highly toxic and some of them are even mutagenic and carcinogenic.<sup>3</sup> Therefore, it is environmentally important to develop options to remove them economically and effectively.

Recently, advanced oxidation processes (AOPs) have been considered as potentially powerful methods and have been the subject of growing interest in wastewater treatment for removing the recalcitrant organics. As one of AOPs, electro-Fenton (EF) has drawn amazing attention as a promissory alternative technology by overcoming some intrinsic drawbacks of traditional Fenton process.<sup>4,5</sup> EF employs electrochemical reactions to generate *in situ* Fenton reagents from eqn (1).<sup>6</sup> Therefore, it is of great advantages since no  $\text{H}_2\text{O}_2$  is needed.

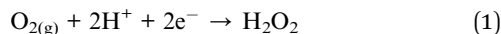
Since  $\cdot\text{OH}$  production does not involve the use of harmful chemicals, this process is environmentally friendly.<sup>7–9</sup> Solid catalyst containing iron species is introduced in the traditional EF to avoid pH adjustment, transforming the homogeneous process into a heterogeneous one.<sup>10,11</sup> In this case, soluble  $\text{Fe}^{2+}$  is replaced by Fe-containing solids.<sup>12</sup> Moreover,  $\text{Fe}^{\text{II}}$  could be regenerated rapidly from the reduction of  $\text{Fe}^{\text{III}}$  at the cathode thanks to the enhancement of electron transfer, which was the limiting step in traditional Fenton process due to low rate constant of  $\text{Fe}^{3+}$  reduction reaction. However, there is a drawback of low efficiency in EF due to the limited cathode surface area. Three-dimensional electrode was proposed as a means of enlarging the electrode surface area by involving particle electrodes since the rate of electrochemical reactions are dependent on electron transfer rate, which is directly proportional to the specific surface area of the electrode.<sup>13</sup> Recently, many studies focuses on the preparation of particle electrodes with high activity and stability to facilitate the application of 3D electrochemical system.<sup>14</sup> Particle electrodes frequently used in 3D electrochemical reactions are dominantly carbonaceous material and metallic material. However, the complicated preparation process and expensive or unavailable raw materials restrict the development of such kind of particle electrodes.<sup>15</sup> EF coupled with three-dimensional electrode could overcome the problem of low current efficiency, as well as give full play to the

Hunan Provincial Key Laboratory of Shale Gas Resource Utilization, School of Civil Engineering, Hunan University of Science and Technology, Xiangtan 411201, China.  
E-mail: h3i3t0@126.com

† Electronic supplementary information (ESI) available. See DOI: 10.1039/c7ra00361g



advantages of both technologies. Catalytic particle electrodes (CPEs) integrated catalyst and particle electrode, and CPEs served both catalyst and particle electrode in 3D EF system. Therefore, it is of great importance to prepare efficient and stable CPEs with available and cost-effective raw materials, which is beneficial to full scale application.<sup>16</sup> The integration of EF and three-dimensional electrode would be bound to induce the acceleration of electrochemical reactions and the improvement of treatment efficiency.



In the current study, SAC-Fe was developed from sewage sludge and iron sludge and served as CPEs to form three-dimensional electrochemical system. SAC-Fe also worked as heterogeneous catalyst in EF to catalyze the decomposition of electro-generated  $\text{H}_2\text{O}_2$ . The corresponding reaction mechanisms at acid and basic conditions were investigated through the role of participant oxidants. Three NHCs were degraded in this 3D EF and the degradation pathways were proposed. Additionally, the relationship between the activity and the structure was explored by the analysis of quantitative structure–activity relationship (QSAR).

## 2. Materials and methods

### 2.1. Chemicals

The NHCs were purchased from Yongda Chemical Reagent Company Ltd (Tianjin, China). HPLC grade methanol and acetic acid were obtained from Fisher Scientific Company (Fair Lawn, USA). All chemicals were analytical grade reagents and were used directly without further purification. All the reaction mediums were deionized water.

### 2.2. Preparation and characterization of CPEs

SAC-Fe was composed of sewage sludge and iron sludge, prepared *via* a one-step method combining the carbonization and Fe-loading process. The facile synthesis process was as follows: first, the dewatered sewage sludge and iron sludge were dried at 105 °C for 24 h, and then ground and sieved into a uniform size of less than 200 mesh. 20 g mixture of sewage sludge and iron sludge samples according to a certain proportion was added into a 150 mL of 3 mol L<sup>−1</sup> ZnCl<sub>2</sub> solution as activation agent (sludge : ZnCl<sub>2</sub> = 1 : 3, by mass). The suspension was stirred for 24 h slowly at ambient temperature, evaporated in a rotary evaporator at 60 °C and dried at 105 °C. Subsequently, the dried solid was pyrolyzed under flowing nitrogen (100 mL min<sup>−1</sup>) in a horizontal quartz furnace at 700 °C for 2 h at a rate of 20 °C min<sup>−1</sup>. The pyrolyzed samples were washed with 3.0 mol L<sup>−1</sup> HCl to rinse the inorganic impurities followed by thoroughly washed with deionized water several times until pH of rinsed water became constant to remove the loosely bonded metal irons. Sewage sludge derived activated carbon (SAC) was prepared without adding iron sludge. Finally the samples were dried at 105 °C and stored in desiccators prior to use.

The main physicochemical properties of CPEs are listed in Table S1.† SAC-Fe and SAC exhibited a high specific surface area more than 350 m<sup>2</sup> g<sup>−1</sup> and showed mesoporous character (Fig. S1†). The main catalytic component of SAC-Fe was Fe<sub>3</sub>O<sub>4</sub> according to the XRD and XPS analysis (Fig. S2 & S3†), providing catalytic sites in EF reaction. The FTIR spectra (Fig. S4, detailed information in ESI†) indicated that chemical bonds between the inorganic compound (SiO<sub>2</sub>) in the sewage sludge and the loaded Fe compound were formed during the carbonization process. The iron oxide was impregnated in the carbon matrix, which was beneficial from the pre-mixture of sewage sludge and iron sludge (iron source). The formation of chemical bands between Fe and carbon matrix, carbonaceous texture, high Fe content and large specific surface area of the as-synthesized SAC-Fe sample guarantee the potential to act as a stable and efficient CPEs and heterogeneous catalyst for the 3D EF system. (More information on the preparation and characterization of SAC-Fe could be obtained in our previous study.<sup>16</sup>)

### 2.3. Experimental procedures

Degradation experiments were conducted in a one-compartment electrochemical cell (1.0 L). The anode was a Pt sheet (4 cm × 5 cm × 0.3 cm) and the cathode was a piece of activated carbon fiber (ACF) with the same dimension. The gap between the electrodes was 4 cm. In a typical run, the as-synthesized CPEs (SAC-Fe and SAC) were filled into NHCs solutions. Then the vessels were shaken for 48 h to ensure the adsorption equilibrium. After equilibrium, the adsorption saturated CPEs were transferred to electrolysis cell. The degradation reaction was initiated by switching on the DC current. Current density and was optimized and maintained at 10 mA cm<sup>−2</sup>, and CPEs dosage was set to be 5.0 g L<sup>−1</sup> (ESI†). Air was bubbled from the bottom of the reactor (4.0 L min<sup>−1</sup>) to provide oxygen and generate stirring in the solution. The reaction temperature was kept at 25 °C by a thermostatic bath. NHCs were degraded in an aqueous medium containing 0.05 M Na<sub>2</sub>SO<sub>4</sub> as supporting electrolyte. The initial concentrations of the three NHCs were 20 mg L<sup>−1</sup>, according to the water quality analysis of coal chemical industry wastewater. Samples were withdrawn at pre-selected time intervals followed by filtered with 0.45 μm filter paper. Then the samples were stored at 4 °C for further analysis.

### 2.4. Analytical methods

NHCs were measured by HPLC equipped with Agilent AQ-C18 column (4.6 mm × 150 mm × 5 μm) and selected photodiode detector. The mobile phase was a mixture of methanol and acetic acid with a flow rate of 1.0 mL min<sup>−1</sup>. Total organic carbon (TOC) was measured with a TOC Analyzer (TOC-CPN, Shimadzu, Japan). For intermediates identification, samples were analyzed by GC-MS followed by extraction with CH<sub>2</sub>Cl<sub>2</sub> and concentrated processes. The organics were determined with an Agilent 6890N gas chromatograph interfaced with a 5973C mass selective detector (MSD) and equipped with an Agilent 7683B auto sampler and a DB5-MS capillary column. Helium was used as the carrier gas with a flow rate of 1.0 mL min<sup>−1</sup>. Hydrogen peroxide generated in the solution was measured with iodide



method.<sup>17</sup> The generation of hydroxyl radicals ( $\cdot\text{OH}$ ) was monitored by means of terephthalic acid (TA) fluorescent probe method on RF-6500 fluorescence spectrometer.<sup>18</sup>

### 3. Results and discussion

#### 3.1. Catalytic performance of 3D EF over wide pH ranges

Fig. 1a illustrates the degradation of NHCs (indole, quinoline and pyridine) in 3D EF with SAC-Fe as CPEs at optimal pH 3.0. NHCs were rapidly degraded in this 3D EF system. The removal efficiencies of indole, quinoline and pyridine achieved 99.1%, 96.7% and 64.2% within 120 min, with the final concentrations of 0.18, 0.66 and 7.16  $\text{mg L}^{-1}$  respectively. The oxidation behavior in 3D EF with the addition of SAC-Fe benefited from not only the properties of iron oxide embedded in SAC-Fe but also by the porous texture of the material. The high degradation efficiencies of NHCs were mostly due to the excellent characteristics of adsorption, conductivity and catalysis of SAC-Fe with extremely high surface area of  $351.6 \text{ m}^2 \text{ g}^{-1}$ , which can efficiently generate  $\text{H}_2\text{O}_2$  during electrochemical process and catalytically decompose  $\text{H}_2\text{O}_2$  to powerful radicals. Microporosity strongly favored the pollutants adsorption capacity and

tended to reduce the metal leaching, while mesoporosity strongly increased the metal dispersion.<sup>12,19</sup> That is why SAC-Fe exhibited efficient catalytic activity in 3D EF. In addition, the kinetic analysis was conducted for NHCs degradation in the 3D EF system. Since the establishment of Fenton system proceeded in the initial period of EF, the degradation process after 20 min was separated for kinetic analysis. The degradations of NHCs were observed to approximately follow a pseudo-first-order kinetic model. The apparent rate constants were determined to be 0.0447, 0.0317 and 0.0097  $\text{min}^{-1}$  for indole, quinoline and pyridine degradations.

TOC was measured to indicate the organic mineralization. TOC removals of NHCs degradation in the 3D EF at a wide pH range of 3.0–10.0 were illustrated in Fig. 1b. TOC removal efficiencies of NHCs degradation decreased slightly ( $\sim 8\%$ ) when increasing pH from 3.0 to 9.0. While a quick decline of TOC removals ( $\sim 12\%$ ) were observed when further raising pH to 10.0. The reasons are mostly due to the fast decomposition of  $\text{H}_2\text{O}_2$  into  $\text{H}_2\text{O}$  and  $\text{O}_2$  at strong basic conditions as well as the decreasing of the adsorption of  $\text{H}_2\text{O}_2$  on the catalyst covered with  $\text{Fe}^{\text{III}}$  complexes.<sup>20</sup> In addition, the oxidation power of radicals weakened as increasing alkalinity. It was demonstrated that the 3D EF with SAC-Fe as CPEs was efficient within wide pH ranges from 3.0 to 9.0 without sacrificing efficiency.

#### 3.2. Reaction mechanism

In order to understand the promotion effect of the prepared CPEs in 3D EF, amounts of electro-generated  $\text{H}_2\text{O}_2$  were measured. It was determined that the corresponding amount of  $\text{H}_2\text{O}_2$  was  $442.7 \mu\text{mol L}^{-1}$  (60 min) with SAC as CPEs, much higher than that ( $259.9 \mu\text{mol L}^{-1}$ ) in 2D system (without CPEs), which demonstrated that the high efficient pollutants removals in 3D EF were mainly related to the more amount of  $\text{H}_2\text{O}_2$  generation. Every pair of CPEs formed a micro-electrolysis cell with the addition of CPEs, transforming it into 3D system. The electrode area and active sites to produce  $\text{H}_2\text{O}_2$  increased multiply, inducing the rise of  $\text{H}_2\text{O}_2$  production accordingly.

Since  $\cdot\text{OH}$  is crucial for understanding the efficiency of EF, amount of  $\cdot\text{OH}$  in this efficient 3D EF system was detected with TA at different pH values. As can be seen from Fig. 2, amount of  $\cdot\text{OH}$  declined notably with extending pH from 3.0 to 9.0. More  $\cdot\text{OH}$  were produced in acid solution than basic condition. However, insignificant decline of TOC removal was observed when increasing pH from 3.0 to 9.0. This observation indicated that the oxidation mechanism of 3D EF with SAC-Fe addition in acid and basic solution would be different. Therefore, participant oxidants generated during the decomposition of  $\text{H}_2\text{O}_2$  by SAC-Fe in acid and basic solution were deeply studied as follows.

Moreover,  $\cdot\text{OH}$  and/or superoxide anion ( $\text{O}_2^{\cdot-}$ ) were the main oxidants generated from the decomposition of  $\text{H}_2\text{O}_2$ . The superoxide anion was the conjugate base of hydroperoxyl radicals ( $\text{HO}_2^{\cdot}$ ) ( $\text{HO}_2^{\cdot} \leftrightarrow \text{H}^+ + \text{O}_2^{\cdot-}$ ). Herein, radical scavengers were employed to investigate the possible role of  $\cdot\text{OH}$  and  $\text{O}_2^{\cdot-}$ . Isopropanol (i-PrOH) has been described as the best  $\cdot\text{OH}$  quencher due to its high rate constant reaction with  $\cdot\text{OH}$

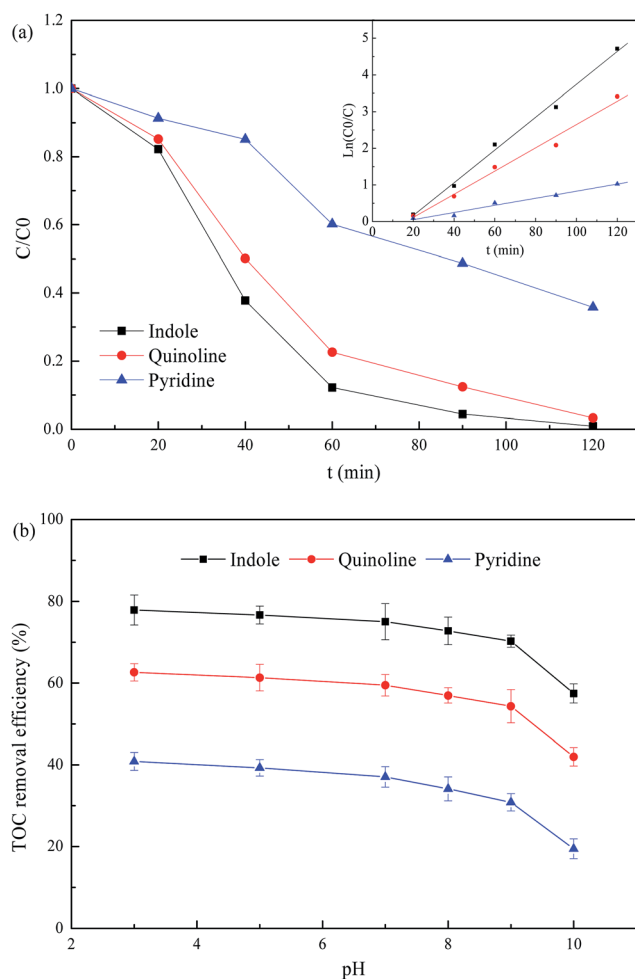


Fig. 1 Catalytic degradation of NHCs and effect of pH on degradation performance in 3D EF.



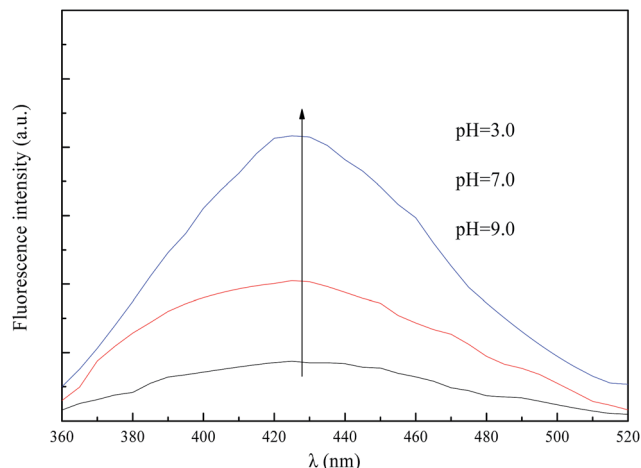


Fig. 2 Fluorescence test for hydroxyl radicals measurement.

$(1.9 \times 10^9 \text{ M}^{-1} \text{ s}^{-1})$ ,<sup>17,21</sup> while benzoquinone (BQ) is known for possessing high ability to trap superoxide anions by a simple electron transfer mechanism.<sup>22,23</sup> As shown in Fig. 3a, higher

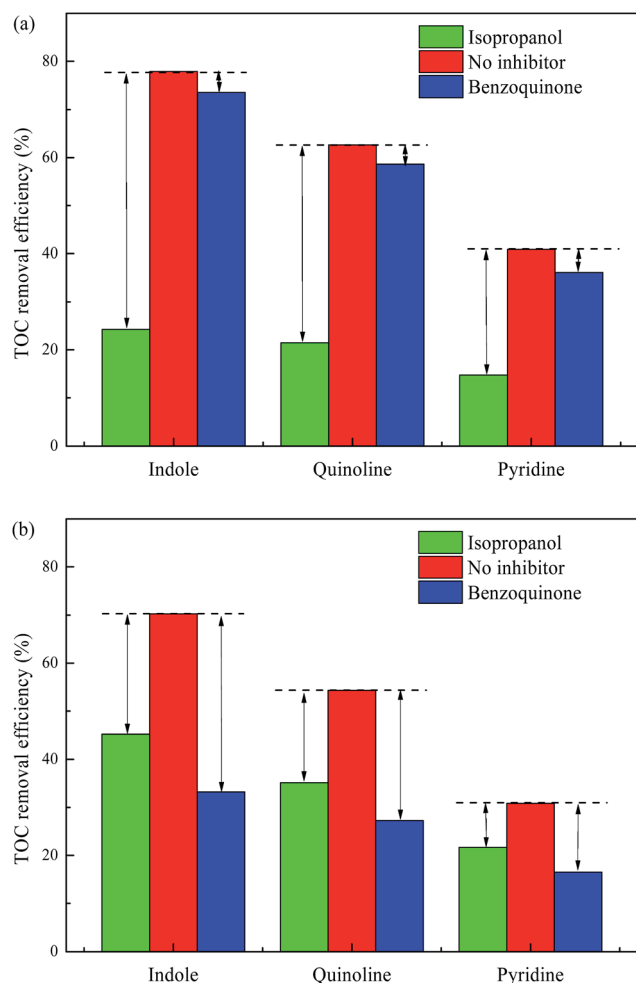


Fig. 3 Effects of scavengers on NHCs degradations ((a) pH = 3.0, (b) pH = 9.0).

inhibition rate was observed in TOC removal at pH 3.0 when i-PrOH was added than BQ. *e.g.* TOC removal efficiency declined 53.62% and 4.37% for indole degradation when radical scavengers of i-PrOH and BQ were added to acid solution at pH 3.0. The significant inhibitory effect of isopropanol suggested that  $\cdot\text{OH}$  presented as main participation under acid conditions. Fig. 3b depicted the influences of radical scavengers on NHCs degradation at pH 9.0. 25.08% and 37.04% inhibition were observed in TOC removal for indole degradation as the addition of i-PrOH and BQ. The results categorically evidenced that different radicals were the main participant oxidants under acid and basic condition. Hydroxyl radical was dominant participant oxidant in acid solution and oxidants generated in 3D EF under basic condition were mainly  $\cdot\text{O}_2^-/\text{HO}_2\cdot$  and to lesser extent were  $\cdot\text{OH}$ .

Since the catalytic site of Fenton reaction was immobilized on the solid CPES, decomposition of  $\text{H}_2\text{O}_2$  was almost completely surface-catalyzed process (stability and reusability tests of SAC-Fe were shown in the ESI†). Based on the above study, the possible reaction mechanism involved in 3D EF with the prepared CPES was proposed and as depicted in Fig. 4. The reaction was possibility initiated by the carbon adsorption. Firstly an abundance of active  $\text{O}_2$  and pollutants were rapidly diffused toward the CPES surface and enriched in diverse size pores of CPES and kept a high local concentration due to the efficient adsorption performance. Then, active  $\text{O}_2$  was reduced to  $\text{H}_2\text{O}_2$  *in situ* via

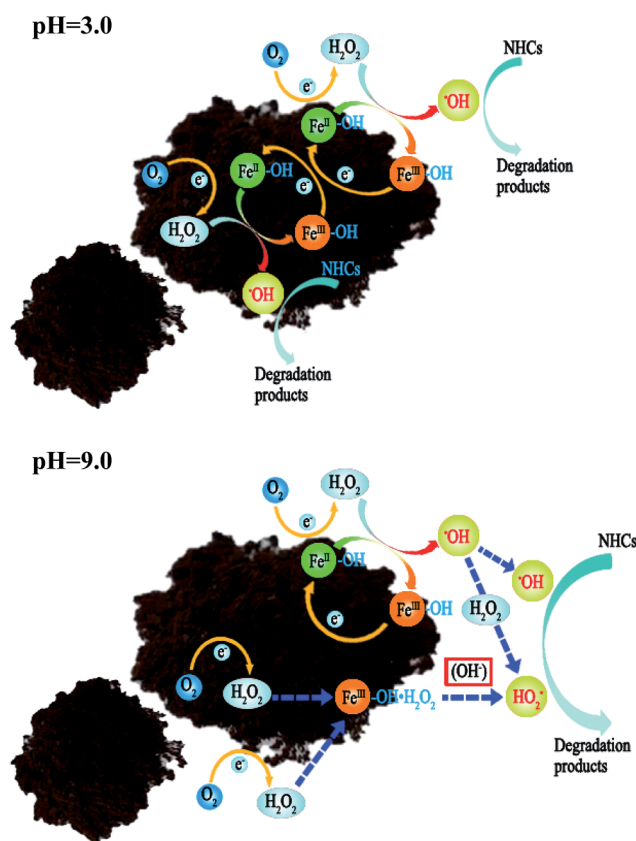


Fig. 4 Schematic illustration of 3D EF reaction mechanisms with SAC-Fe in acidic and basic condition.

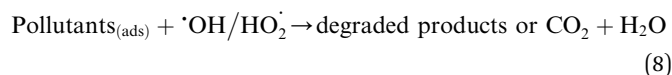
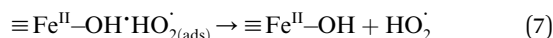
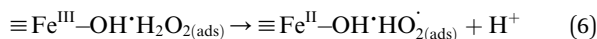
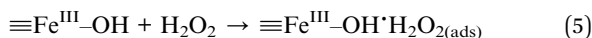
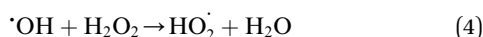
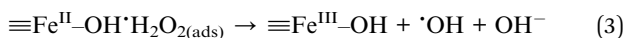
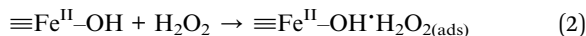




two-electron reduction on the interface between CPEs and the bulk phase. It was reported that heterogeneous Fenton reaction began with the adsorption of  $\text{H}_2\text{O}_2$  molecules on the hydrated catalyst.<sup>24</sup>

In acidic solution, once  $\text{H}_2\text{O}_2$  molecules were generated on the CPEs, it would be catalytically decomposed to strong oxidizer  $\cdot\text{OH}$  radicals by embedded iron oxide on the surface and internal of the CPEs promptly, presumably through a Haber–Weiss mechanism. Finally, the NHCs were degraded even mineralized by the generated  $\cdot\text{OH}$ .

In basic solution, the interaction of  $\text{H}_2\text{O}_2$  with the catalytic sites ( $\text{Fe}^{\text{III}}$  and  $\text{Fe}^{\text{II}}$ ) on the SAC-Fe surface was expected.<sup>22</sup> Based on the above analysis, a surface-based mechanism different from in acidic condition was proposed. The electro-generated  $\text{H}_2\text{O}_2$  interacted with surface iron species ( $\text{Fe}^{\text{III}}\text{--OH}$  and  $\text{Fe}^{\text{II}}\text{--OH}$ ) of the hydrated surface. For  $\text{Fe}^{\text{II}}\text{--OH}$ , it reacted with  $\text{H}_2\text{O}_2$  to  $\text{Fe}^{\text{III}}\text{--OH}$  and  $\cdot\text{OH}$  (eqn (2) and (3)). Meanwhile, most of generated  $\cdot\text{OH}$  in first stage would be scavenged by considerable  $\text{H}_2\text{O}_2$  at the immediate vicinity (eqn (4)). For  $\text{Fe}^{\text{III}}\text{--OH}$ , it interacted with  $\text{H}_2\text{O}_2$  to form a precursor surface complex of  $\text{H}_2\text{O}_2$  (eqn (5)). The surface  $\text{H}_2\text{O}_2$  complex may further undergo a reversible ground-state electron transfer from ligand to metal (eqn (6)), and then the successor complex deactivated *via* eqn (7) to release  $\text{HO}_2\cdot$  oxidants.<sup>22,25</sup> It was noted that reaction (6) would be more active in basic solution since hydroxyl ions can react with the formed protons from reaction (5) promptly, promoting the forward reaction. The  $\text{Fe}^{\text{II}}\text{--OH}$  and  $\text{Fe}^{\text{III}}\text{--OH}$  recycled *via* reaction (3), (6) and (7). That is why participant oxidants generated in 3D EF at pH 9.0 were mainly  $\text{HO}_2\cdot$  and to lesser extent were  $\cdot\text{OH}$ .



The formed radicals then reacted with the contaminants and degraded those compounds into intermediates or complete mineralization (eqn (8)). Since the contaminants were enriched on the CPEs resulting from adsorption effect and maintained at high concentration, these pollutants *in situ* captured radicals and improved radicals utilization.

Abundant iron species embedded in porous CPEs with high exposure endowed more catalytic active sites. Fe species were impregnated in the carbon matrix obtained from the pyrolysis process, preventing the iron from aggregating into clusters and exhibiting better decentrality both on the surface and internally in the CPEs, which resulted in the improvement in the number

and properties of the reactive surface sites to promote radicals production. Thus, the efficient degradation of NHCs was realized.

### 3.3. Degradation pathway

The changes of UV-Vis spectra in the degradations of NHCs were illustrated in Fig. 5. A continuous decrease at 256 nm was

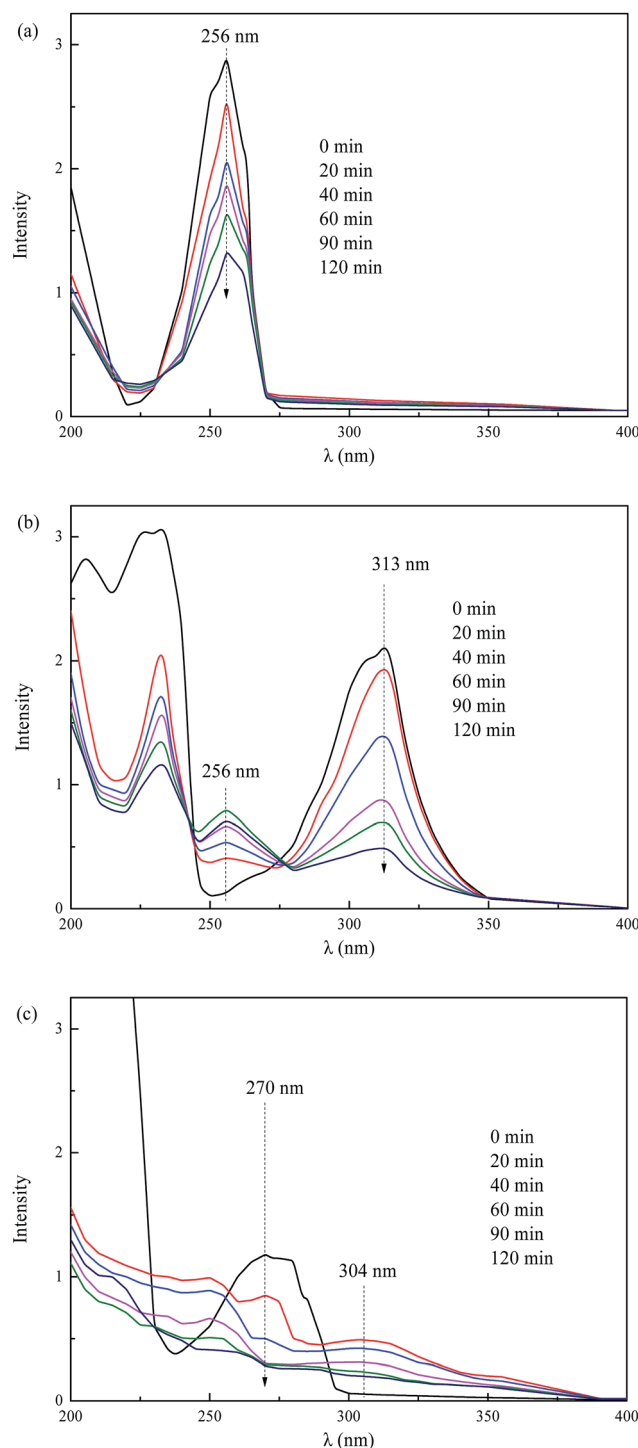


Fig. 5 Variations of UV-Vis spectra in the degradation of NHCs. ((a) Pyridine, (b) quinoline, (c) indole.)



observed for pyridine degradation (Fig. 5a), indicating the decomposition of pyridine. For quinoline degradation, the adsorption peak at 313 nm declined rapidly in 60 min, demonstrating the fast degradation of quinoline (Fig. 5b). The peak appeared at around 256 nm suggested that intermediates analogous to the structure of pyridine were formed in the degradation of quinoline. A quick decline at 270 nm was found in indole degradation (Fig. 5c). Other peaks emerged at around 245–260 nm and 304 nm evidenced the generation of considerable intermediates. The main intermediates in the degradations of NHCs were listed in Table 1. Pyridine is one kind of NHCs lack of  $\pi$  electron. In the structure of pyridine, the pair of electrons at the nitrogen atom does not conjugate with the ring, and the nitrogen atom attracts electrons and deactivates the ring, since the electron cloud density of the ring is low

resulted from the attraction of nitrogen atom.<sup>26</sup> The cloud density of the meta carbon atom is higher than others, and the meta carbon atom is prone to electrophile substitution reaction. In the structure of quinoline, the isolated pair of electrons at the nitrogen atom does not conjugate with the heterocyclic ring, inducing the higher cloud density on the benzene ring. This structure reduces the reactivity of the heterocyclic ring to electrophile reagent and enhances the reactivity of the benzene ring instead. The electrophile attack occurs readily on the benzene ring. The pyrrole ring of indole is super  $\pi$  electron structure, causing the high reactivity of the pyrrole ring due to its high cloud density. Based on the structure analysis of NHCs and the intermediates detections, the degradation pathways of NHCs by the 3D EF oxidation were proposed in Fig. 6.

**Table 1** Observed organic intermediates in NHCs degradations

NHCs	Observed intermediates
Pyridine	3-Hydroxypyridine, 2,3-dihydroxypyridine, 2(2H)-pyridinone-one, 2N hexadiene dicarboxaldehyde, succinate
Quinoline	5-Hydroxyquinoline, 8-hydroxyquinoline, 5,8-dihydroxyquinoline, pyridine-2,3-diglyoxylate acid, pyridine-2,3-dicarboxaldehyde, pyridine-2,3-dicarboxylic acid, pyridine-2-carboxyl-3-carboxaldehyde, pyridine-3-carboxyl-2-carboxaldehyde, 3-carboxypyridine, 2-carboxypyridine, succinate, formic acid
Indole	Isatin, <i>o</i> -aminobenzoic acid, oxalic acid, propionic acid, acetic acid

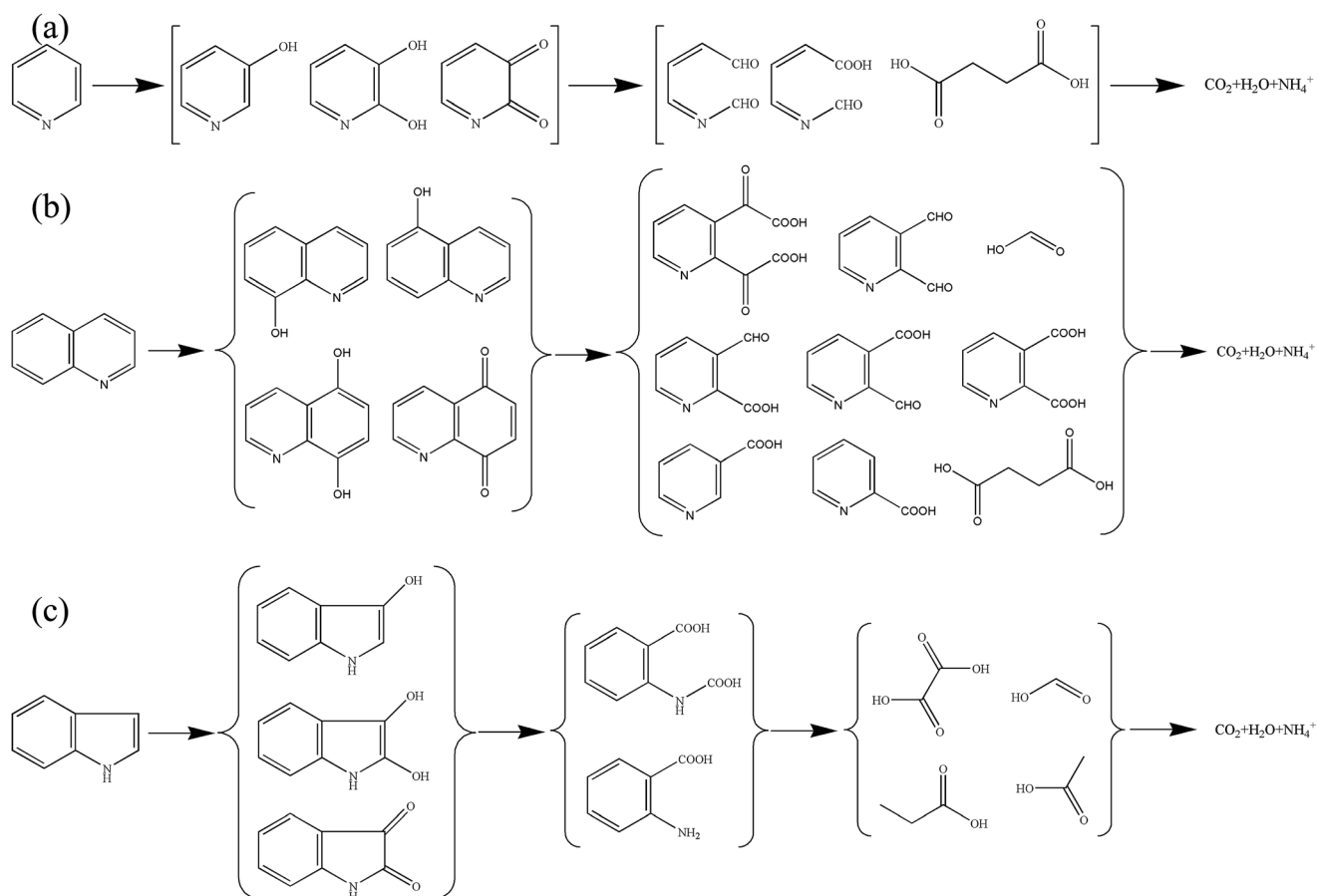


**Fig. 6** Possible degradation pathways of the three NHCs. (a) Pyridine, (b) quinoline, (c) indole.



Table 2 Theoretical descriptors of NHCs (eV)

NHCs	$E_{\text{HOMO}}$	$E_{\text{LUMO}}$	$E_{\text{LUMO}} - E_{\text{HOMO}}$
Pyridine	−10.036	0.609	10.645
Quinoline	−9.003	0.145	9.148
Indole	−8.355	0.173	8.528
Isoquinoline	−8.825	0.032	8.857

### 3.4. QSAR

Significant differences were observed in the degradations of the above three NHCs. Compound structure determines the degradation properties, so it was meaningful to explore the relationship between the degradation rates and the pollutant structure. The pseudo-first-order rate constants of the NHCs were calculated in Section 3.1 (Fig. 1). The degradation rates of the three NHCs by 3D EF in decline order were indole > quinoline > pyridine. In order to explore the relationship between the structure and activity, a QSAR analysis was performed. The quantum descriptors used were  $E_{\text{HOMO}}$ ,  $E_{\text{LUMO}}$  and  $E_{\text{LUMO}} - E_{\text{HOMO}}$  (Table 2). These descriptors reflect the character of oxidation/reduction of the compounds.<sup>27,28</sup> The QSAR model was obtained from the stepwise variance regression of  $\ln k_a$  and the descriptors (eqn (9)). The polynomial regression model produced high squared correlation coefficient ( $R^2 = 0.9947$ ), corroborating the high precision and reliability of the developed QSAR model to describe the relationship between the degradation properties and the compound structures. An increase of  $E_{\text{LUMO}} - E_{\text{HOMO}}$  led to a decrease of degradation rate, and the low  $E_{\text{HOMO}}$  had adverse effect on the degradation. The compound with a high value of  $E_{\text{LUMO}} - E_{\text{HOMO}}$  implies that electrophile attack is restricted.<sup>29,30</sup> The attack of  $\cdot\text{OH}$  is electrophile reaction. For example,  $E_{\text{LUMO}} - E_{\text{HOMO}}$  of pyridine is highest among these NHCs, so the electrophile attack takes place difficultly. The developed QSAR model was validated by the degradation of isoquinoline. The apparent rate constants of isoquinoline degraded by 3D EF and calculated from the model were 0.0372 and 0.0383  $\text{min}^{-1}$  respectively, further evidencing the accuracy of the model. The results provided an insight to the relationship between the degradation of the NHCs and their structures.

$$\ln k_a = -0.64102 \times (E_{\text{LUMO}} - E_{\text{HOMO}}) - 0.38264 \times E_{\text{LUMO}} + 2.42808 \quad (9)$$

## 4. Conclusions

This study reported a three-dimensional heterogeneous electro-Fenton system with SAC-Fe as CPEs. This 3D EF system worked very well over a wide pH ranges from 3.0 to 9.0 without sacrificing efficiency. SAC-Fe worked not only as CPEs for efficiently *in situ* electro-generating  $\text{H}_2\text{O}_2$ , but also as heterogeneous catalyst for catalytically decomposing  $\text{H}_2\text{O}_2$  to produce radicals. The corresponding reaction mechanisms of the 3D EF on the CPEs at different pH ranges were proposed by employing

radicals scavengers. In acidic solution,  $\cdot\text{OH}$  was the dominant participant oxidant, following a Haber-Weiss mechanism.  $\text{Fe}^{\text{II}}$  sites on SAC-Fe catalyzed the decomposition of  $\text{H}_2\text{O}_2$  to generate  $\cdot\text{OH}$ . While in basic solution, the oxidants generated from the decomposition of  $\text{H}_2\text{O}_2$  were mainly  $\cdot\text{O}_2^-/\text{HO}_2\cdot$  and to lesser extent were  $\cdot\text{OH}$ . The formation and decomposition of  $\text{H}_2\text{O}_2$  complex with catalytic sites ( $\text{Fe}^{\text{II}}$  and  $\text{Fe}^{\text{III}}$ ) as well as the catalytic decomposition of  $\text{H}_2\text{O}_2$  were involved in the catalytic reactions to generate  $\cdot\text{O}_2^-/\text{HO}_2\cdot$  and  $\cdot\text{OH}$ . Possible degradation pathways of NHCs were proposed as well. A QSAR model was developed to describe the relationship between degradation properties of NHCs and their structures. This promising 3D EF has great development potential for practical wastewater treatment since its high efficiency and friendly working condition especially at neutral pH. And the understanding of the catalytic oxidation mechanism may lead to the development of more efficient CPEs and optimization of the process parameters.

## Acknowledgements

This work was supported by the National Natural Science Foundation of China (No. 41472328 and No. 41672350) and the scientific research project of Hunan Provincial Education Department (No. 15C0556).

## References

- 1 F. Sun, Q. Yu, J. Zhu, L. Lei, Z. Li and X. Zhang, *Chemosphere*, 2015, **134**, 402–407.
- 2 P. Xu, H. Han, H. Zhuang, B. Hou, S. Jia, D. Wang, K. Li and Q. Zhao, *J. Environ. Sci.*, 2015, **31**, 221–225.
- 3 P. Liao, S. Yuan, W. Xie, W. Zhang, M. Tong and K. Wang, *J. Colloid Interface Sci.*, 2013, **390**, 189–195.
- 4 B. Hou, W. Ma, H. Han, P. Xu, H. Zhuang and K. Li, *Desalin. Water Treat.*, 2016, **57**, 8174–8182.
- 5 H. Y. Zhao, L. Qian, X. H. Guan, D. L. Wu and G. H. Zhao, *Environ. Sci. Technol.*, 2016, **50**, 5225–5233.
- 6 E. Bocos, M. Pazos and M. A. Sanroman, *RSC Adv.*, 2016, **6**, 1958–1965.
- 7 A. Ozcan, Y. Sahin and M. A. Oturan, *Water Res.*, 2013, **47**, 1470–1479.
- 8 W. R. P. Barros, P. C. Franco, J. R. Steter, R. S. Rocha and M. R. V. Lanza, *J. Electroanal. Chem.*, 2014, **722**, 46–53.
- 9 E. Alfaya, O. Iglesias, M. Pazos and M. A. Sanroman, *RSC Adv.*, 2015, **5**, 14416–14424.
- 10 E. G. Garrido-Ramirez, M. L. Mora, J. F. Marco and M. S. Ureta-Zanartu, *Appl. Clay Sci.*, 2013, **86**, 153–161.
- 11 Y. B. Wang, H. Y. Zhao and G. H. Zhao, *Appl. Catal., B*, 2015, **164**, 396–406.
- 12 L. Bounab, O. Iglesias, E. Gonzalez-Romero, M. Pazos and M. A. Sanroman, *RSC Adv.*, 2015, **5**, 31049–31056.
- 13 C. H. Zhang, H. Lin, J. Chen and W. W. Zhang, *Environ. Technol.*, 2013, **34**, 2371–2376.
- 14 B. Hou, H. Han, H. Zhuang, P. Xu, S. Jia and K. Li, *Bioresour. Technol.*, 2015, **196**, 721–725.
- 15 Z. Y. Wang, J. Y. Qi, Y. Feng, K. Li and X. Li, *J. Ind. Eng. Chem.*, 2014, **20**, 3672–3677.



- 16 B. Hou, H. Han, S. Jia, H. Zhuang, P. Xu and K. Li, *J. Taiwan Inst. Chem. Eng.*, 2016, **60**, 352–360.
- 17 S. Qiu, D. He, J. X. Ma, T. X. Liu and T. D. Waite, *Electrochim. Acta*, 2015, **176**, 51–58.
- 18 X. W. Cheng, Q. F. Cheng, X. Y. Deng, P. Wang and H. L. Liu, *Electrochim. Acta*, 2015, **184**, 264–275.
- 19 H. Y. Zhao, Y. Chen, Q. S. Peng, Q. N. Wang and G. H. Zhao, *Appl. Catal., B*, 2017, **203**, 127–137.
- 20 Y. Wang, Y. K. Sun, W. G. Li, W. D. Tian and A. Irini, *Chem. Eng. J.*, 2015, **267**, 1–8.
- 21 L. Lyu, L. Zhang and C. Hu, *Chem. Eng. J.*, 2015, **274**, 298–306.
- 22 W. G. Li, Y. Wang and A. Irini, *Chem. Eng. J.*, 2014, **244**, 1–8.
- 23 O. Scialdone, A. Galia, C. Gattuso, S. Sabatino and B. Schiavo, *Electrochim. Acta*, 2015, **182**, 775–780.
- 24 L. Gu, N. W. Zhu, H. Q. Guo, S. Q. Huang, Z. Y. Lou and H. P. Yuan, *J. Hazard. Mater.*, 2013, **246**, 145–153.
- 25 L. Gu, N. W. Zhu and P. Zhou, *Bioresour. Technol.*, 2012, **118**, 638–642.
- 26 H. Zhao, S. H. Xu, J. B. Zhong and X. H. Bao, *Catal. Today*, 2004, **93–5**, 857–861.
- 27 H. Kusic, B. Rasulev, D. Leszczynska, J. Leszczynski and N. Koprivanac, *Chemosphere*, 2009, **75**, 1128–1134.
- 28 H. C. Zhu, Z. M. Shen, Q. L. Tang, W. C. Ji and L. J. Jia, *Chem. Eng. J.*, 2014, **255**, 431–436.
- 29 L. J. Jia, Z. M. Shen, W. M. Guo, Y. A. Zhang, H. C. Zhu, W. C. Ji and M. H. Fan, *J. Taiwan Inst. Chem. Eng.*, 2015, **46**, 140–147.
- 30 H. C. Zhu, W. M. Guo, Z. M. Shen, Q. L. Tang, W. C. Ji and L. J. Jia, *Chemosphere*, 2015, **119**, 65–71.

